



HAL
open science

Light and thermally activated spin crossover coupled to an order–disorder transition of a propyl chain in an iron(III) complex

Theerapoom Boonprab, Upeksha Habarakada, Guillaume Chastanet, Phimpaka Harding, David Harding

► To cite this version:

Theerapoom Boonprab, Upeksha Habarakada, Guillaume Chastanet, Phimpaka Harding, David Harding. Light and thermally activated spin crossover coupled to an order–disorder transition of a propyl chain in an iron(III) complex. *CrystEngComm*, 2023, 25 (29), pp.4126-4132. 10.1039/d3ce00425b . hal-04171438

HAL Id: hal-04171438

<https://hal.science/hal-04171438v1>

Submitted on 27 Jul 2023

HAL is a multi-disciplinary open access archive for the deposit and dissemination of scientific research documents, whether they are published or not. The documents may come from teaching and research institutions in France or abroad, or from public or private research centers.

L'archive ouverte pluridisciplinaire **HAL**, est destinée au dépôt et à la diffusion de documents scientifiques de niveau recherche, publiés ou non, émanant des établissements d'enseignement et de recherche français ou étrangers, des laboratoires publics ou privés.

Light and thermally activated spin crossover coupled to an order–disorder transition of a propyl chain in an iron(III) complex†

Theerapoom Boonprab,^a Upeksha Habarakada,^b Guillaume Chastanet,^c Phimpaka Harding^{†*a} and David J. Harding^{†*a}

A series of three solvates [Fe(naphPren)₂]*l*·CH₂Cl₂ **1**, [Fe(naphPren)₂]*l*·CHCl₃ **2** and [Fe(naphPren)₂]*l*·acetone **3** with the novel ligand HnaphPren (2-(((2-(propylamino)ethyl)imino)methyl)naphthalen-2-ol) is reported. Magnetic studies of these complexes reveal that **1** exhibits an abrupt SCO at 162 K, whereas **2** possesses a more gradual SCO centred at 172 K. **3** is trapped in the HS state, but irradiation at 980 nm enables accessibility to a hidden LS state via reverse-LIESST. The structures of **1–3** reveal that **1** and **2** show reversible disorder in the propyl group that is coupled to SCO which is absent in the acetone solvate. This study demonstrates how solvent subtly alters the packing impacting the potential flexibility of the propyl chain and thereby switching SCO on or off.

DOI: 10.1039/XXXXXXXXXX

Introduction

Spin crossover (SCO) materials exhibit a reversible spin-transition between the high- and low-spin state upon application of an external stimulus including temperature, pressure or light irradiation.^{1–4} This can occur in d⁴–d⁷ transition metal complexes in which the two spin states are close in energy. Among these, Fe(III) spin crossover compounds are promising, owing to their robustness, an increasingly large number of hysteretic SCO systems, and demonstrated use in devices.^{5–9} Nevertheless, the development of light activated Fe(III) SCO materials through the LIESST effect (Light-Induced Excited Spin-State Trapping) remains challenging due to the smaller change in Fe–ligand bond lengths compared to Fe(II) systems.^{10,11} To date, only handful of ligand systems has been found to support LIESST including pap (pap = 2-((pyridin-2-ylmethylene)amino)phenolate),¹² qnal (qnal = 1-((quinolin-8-ylimino)methyl)naphthalen-2-olate),^{13–16} azp (azp = 2,2'-(diazene-1,2-diyl)

diphenolate),¹⁷ qsal (qsal = 2-((quinolin-8-ylimino)methyl)phenolate)¹⁸ and naphBzen (naphBzen = 1-(((2-(benzylamino)ethyl)imino)methyl)naphthalen-2-olate).⁸

Despite this there appears to be no real correlation between the abruptness of SCO or the presence of hysteresis and light activated SCO, and the discovery of new systems continues to be largely serendipitous.

Abrupt spin crossover occurs when there is strong cooperativity between the spin centres, aided by supramolecular interactions. In some cases, it can also be tied to order–disorder transitions in either the anions^{19–21} or parts of the ligand.^{19,22–24} One of the first examples was in 2003 in [Fe(2-picolyamine)₃](Cl)₂ where an order–disorder transformation coupled to the spin state change resulted in stepped SCO.²⁵ In systems with alkyl groups such as [Fe(*n*-Bu-im)₃(tren)](PF₆)₂ the unusually long relaxation time of the LIESST activated HS state is intimately tied to an order–disorder transition in two of the butyl groups.²² This demonstrates that, not only the abruptness of SCO, with or without hysteresis, but also the LIESST properties can be influenced by such order–disorder changes.

Tridentate ligands such as HsalRen (2-(((2-(*R*-amino)ethyl)imino)methyl)phenol) are among the most common in Fe(III) SCO complexes. Complexes of this family feature intermediate HS–LS states,^{26–28} abrupt SCO,^{27,29,30} abrupt SCO with hysteresis,³⁰ thermosalient behaviour,^{31,32} near room temperature SCO^{33,34} and even hidden hysteresis.⁸ An attractive feature of salRen complexes is that the N–H···anion interaction is predictable and robust and the group on the amine can be readily modified. Despite this, most reported compounds use the ethyl group such as [Fe(naphEen)₂]⁺

^a Department of Chemistry, Institute of Science, Suranaree University of Technology, Nakhon Ratchasima, 30000, Thailand. E-mail: david@g.sut.ac.th, phimpaka@g.sut.ac.th

^b Functional Materials and Nanotechnology Centre of Excellence, Walailak University, Thasala, Nakhon Si Thammarat, 80160, Thailand

^c Université de Bordeaux, CNRS, Bordeaux INP, ICMCB, 87 avenue du Dr A. Schweitzer, Pessac, F-33608, France

† Electronic supplementary information (ESI) available. CCDC 2259253–2259259. For ESI and crystallographic data in CIF or other electronic format see DOI: <https://doi.org/10.1039/d3ce00425b>

‡ Previous address: Functional Materials and Nanotechnology Centre of Excellence, Walailak University, Thasala, Nakhon Si Thammarat, 80160, Thailand.

complexes (naphEen = 1-[[2-(ethylamino)ethylimino]methyl]-2-naphtholate) which are trapped in the LS state.³⁵ In contrast, use of a benzyl group allows access to $[\text{Fe}(\text{naphBzen})_2]^+$ complexes which exhibit a range of hysteretic and gradual SCO behaviour.^{8,36} It follows that further exploration of the impact of the alkyl group is warranted. In this work, we report the synthesis and characterization of $[\text{Fe}(\text{naphPren})_2]\text{I}$ (naphPren = 1-[[2-(propylamino)ethylimino]methyl]-2-naphtholate) which was recrystallized to yield three different solvates; CH_2Cl_2 **1**, CHCl_3 , **2**, and acetone **3**. We demonstrate that the thermo- and photo-induced properties of the compounds are solvent dependent with thermal SCO coupled to an order-disorder transition in the propyl chain.

Experimental section

Materials

All reactions were carried out in aerobic conditions using commercial grade solvents for the synthesis of all compounds. All chemicals were purchased from TCI Chemicals or Sigma-Aldrich and used as received.

Synthesis of $[\text{Fe}(\text{naphPren})_2]\text{I}\cdot\text{CH}_2\text{Cl}_2$ **1**

A solution of 2-hydroxy-1-naphthaldehyde (344.5 mg, 2.0 mmol) in EtOH (3 mL) was charged with *N*-propylethylenediamine (204.4 μL , 2.0 mmol) and stirred under ambient conditions for 1 h. 1,8-diazabicyclo[5.4.0]undec-7-ene, DBU (150 μL , 2.0 mmol) was then added and the resulting mixture was stirred for a further 15 minutes. A solution of $\text{Fe}(\text{NO}_3)_3\cdot 9\text{H}_2\text{O}$ (0.403 g, 1.0 mmol) in EtOH (3 mL) was added dropwise. The solution turned green immediately indicating formation of $[\text{Fe}(\text{naphPren})_2]\text{NO}_3$ and intensified over 15 minutes. The reaction mixture was left stirring for 1 h, before heating to 60 °C. A solution of Potassium iodide (415 mg, 3.0 mmol) in EtOH (14 mL) was added and the solution stirred at this temperature in a sealed vessel for 2 h. The resulting reaction mixture was then allowed to cool to room temperature and stirred for a further 16 h. The crude solution was reduced *in vacuo* to 3 mL and a green solid precipitated with addition of distilled water (5 mL). The green suspension was filtered through a Buchner funnel and dried in air for 2 h. The greenish brown powder of $[\text{Fe}(\text{naphPren})_2]\text{I}$ was then recrystallized *via* slow evaporation from 1:1 CH_2Cl_2 :hexane over 14 days to produce $[\text{Fe}(\text{naphPren})_2]\text{I}\cdot\text{CH}_2\text{Cl}_2$, **1** as black crystals (173 mg, 50% over 2 steps). IR spectroscopy: 3105 ($\nu\text{N-H}$), 2961, 2930, 2871 ($\nu\text{C-H}$), 1608 ($\nu\text{C=N}$). UV-visible absorption (CH_2Cl_2): 603 nm (2512 $\text{M}^{-1}\text{cm}^{-1}$), 695 nm (3336 $\text{M}^{-1}\text{cm}^{-1}$). Elemental analysis: $\text{C}_{32}\text{H}_{38}\text{FeIN}_4\text{O}_2\cdot\text{CH}_2\text{Cl}_2$ theoretical: C (50.92), H (5.18), N (7.20) Experimental: C (50.83), H (5.23), N (7.40).

Synthesis of $[\text{Fe}(\text{naphPren})_2]\text{I}\cdot\text{CHCl}_3$ **2**

Black crystals of **1** (60 mg) were dissolved in CHCl_3 (2 mL) and filtered through a pad of Celite® into a sealable vial. The

solution was then layered above with hexane (10 mL). The vial was sealed and left at room temperature to complete slow diffusion. After 7 days, black crystals of $[\text{Fe}(\text{naphPren})_2]\text{I}\cdot\text{CHCl}_3$ **2** formed and were collected (51 mg, 85%). IR spectroscopy: 3115 ($\nu\text{N-H}$), 2961, 2929, 2870 ($\nu\text{C-H}$), 1612 ($\nu\text{C=N}$). Elemental analysis: $\text{C}_{32}\text{H}_{38}\text{FeIN}_4\text{O}_2\cdot\text{CHCl}_3$ theoretical: C (48.77), H (4.84), N (6.89) Experimental: C (48.44), H (4.90), N (6.72).

Synthesis of $[\text{Fe}(\text{naphPren})_2]\text{I}\cdot\text{acetone}$ **3**

Black crystals of **1** (50 mg) were dissolved in acetone (2 mL) and filtered through pad of Celite® into a sealable vial. The solution was then sealed in a container of Et_2O (5 mL) and left at room temperature to complete slow evaporation-diffusion. After 10 days, black crystals of $[\text{Fe}(\text{naphPren})_2]\text{I}\cdot\text{acetone}$ **3** formed and were collected (34.5 mg, 69%). IR spectroscopy: 3066 ($\nu\text{N-H}$), 2964, 2933, 2871 ($\nu\text{C-H}$), 1616 ($\nu\text{C=N}$), 1533, 1508 ($\nu\text{C=C}$). Elemental analysis: $\text{C}_{32}\text{H}_{38}\text{FeIN}_4\text{O}_2\cdot\text{C}_2\text{H}_6\text{O}$ theoretical: C (55.22), H (6.00), N (7.58) Experimental: C (55.39), H (5.85), N (7.81).

Physical measurements

Infrared spectra (4000–400 cm^{-1}) were recorded as KBr pellets on a Bruker Tensor 27 FT-IR spectrometer with OPUS data collection program (Table S1; Fig. S1†). Absorption spectra was collected on PG Instruments T80+ UV/vis spectrometer from a solution of **1** in CH_2Cl_2 (Fig. S2†) elemental analyses were carried out by using a Eurovector EA3000 analyzer. ESI-MS were carried out on a Bruker AmaZon X LCMS Mass Spectrometer. Thermogravimetric analyses were performed on Mettler Toledo TGA/DSC1 in the range of 35–300 °C (Fig. S3†). Magnetic measurements were carried out with a Quantum Design SQUID MPMS 7XL device operating from 10 K to 300 K at 20 kOe of applied magnetic field. A known amount of freshly recrystallized crystals was introduced into a polypropylene bag whose diamagnetic contribution is known. The temperature scan rate was fixed at 0.5 K min^{-1} from 10 K to 300 K after a fast cooling from room temperature. The diamagnetic corrections for the measured compounds were estimated from Pascal tables. For the photomagnetic measurements, a thin layer of these samples was irradiated in the SQUID magnetometer using an optical fiber guiding the light with a given wavelength onto the sample.

X-ray crystallography

The diffraction data of **1–3** were collected on a Rigaku SuperNova diffractometer with a HyPix 3000 detector using $\text{CuK}\alpha$ radiation ($\lambda = 1.54184 \text{ \AA}$)³⁷ at the temperatures indicated in the ESI† (Table S2). Data reduction, scaling, and absorption corrections were performed using CrysAlisPro.³⁸ The structures were solved, and the space group $P2_1/c$ was determined by intrinsic phasing using ShelXT and refined by full matrix least-squares minimization on F^2 using SHELXL.^{39,40} All non-hydrogen atoms were refined anisotropically. Disorder was found in the propyl groups of **1**

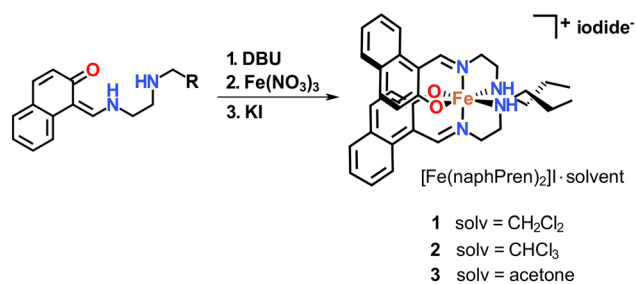
and **2** at higher temperatures and these were modelled in two parts with appropriate SADI and RIGU restraints. In the case of **1**, the CH₂Cl₂ molecule was also found to be disordered at 200 K and similar restraints were used to model this disorder. Hydrogen atoms were included in calculated positions and refined with isotropic thermal parameters, which were 1.2× or 1.5× the equivalent isotropic thermal parameters of their parent carbon or oxygen atoms. All pictures were generated with OLEX2.⁴¹ Crystallographic data for the structures have been deposited with the Cambridge Crystallographic Data Centre (CCDC) 2259253–2259259. Powder X-ray diffraction data were measured on a Rigaku SuperNova diffractometer with a HyPix 3000 detector using Cu K α radiation ($\lambda = 1.54184 \text{ \AA}$). The samples were ground and then suspended in Fomblim Y oil, and the data were collected between $2\theta = 5\text{--}80^\circ$.

Results and discussion

Synthesis and characterization

The Schiff base ligand, HnaphPren was prepared in a similar manner to HnaphEen and HnaphBzen and used *in situ*.^{8,35} The synthesis of [Fe(naphPren)₂]I was made in good yield *via* post-complexation anionic exchange from the nitrate complex as shown in Scheme 1. The resulting green solid was purified by recrystallization from CH₂Cl₂:hexane to yield [Fe(naphPren)₂]I·CH₂Cl₂ **1**. In order to study impact of solvent, **1** was also recrystallized by slow diffusion from either CHCl₃:hexane or acetone:Et₂O to yield [Fe(naphPren)₂]I·CHCl₃ **2** and [Fe(naphPren)₂]I·acetone **3**, respectively. All compounds were characterized by IR and UV-visible spectroscopy, mass spectrometry (Fig. S4 and S5[†]), elemental analysis, and TGA (Fig. S3[†]). In all cases the results are consistent with the proposed degree of solvation.

IR spectroscopy of **1–3** shows peaks corresponding to the amino group, aromatic rings, aliphatic backbone and coordinating imine (Table S1, Fig. S1[†]). The imine stretch is observed between 1609–1614 cm⁻¹ and close to that of [Fe(naphEen)₂]halide,³⁵ but significantly lower than [Fe(naphBzen)₂]I.⁸ This might reflect the different electron donating efficacy of the amine for the benzyl and aliphatic propyl group in these structures. The absorption spectra of **1** in CH₂Cl₂ exhibits a broad peak at 695 nm, matching the LMCT band reported in [Fe(naphEen)₂]halide^{35,42} (Table S1, Fig. S2[†]).



Scheme 1 Synthesis of **1–3**.

The position of λ_{max} is consistent with LS Fe(III) as found in a range of [Fe(salRen)₂]⁺ and [Fe(naphRen)₂]⁺ complexes.

Magnetic measurements

The spin crossover profiles of **1–3** were determined by SQUID magnetometry and are shown as $\chi_M T$ vs. temperature plots in Fig. 1 (χ_M being the molar magnetic susceptibility). In **1** below 140 K $\chi_M T \approx 0.4 \text{ cm}^3 \text{ mol}^{-1} \text{ K}$, corresponding to LS Fe(III). Heating results in an abrupt SCO with $\chi_M T$ reaching $3 \text{ cm}^3 \text{ mol}^{-1} \text{ K}$ at 165 K, before levelling out to $4.1 \text{ cm}^3 \text{ mol}^{-1} \text{ K}$, corresponding to HS Fe(III) after 220 K, giving a $T_{1/2} = 162 \text{ K}$.

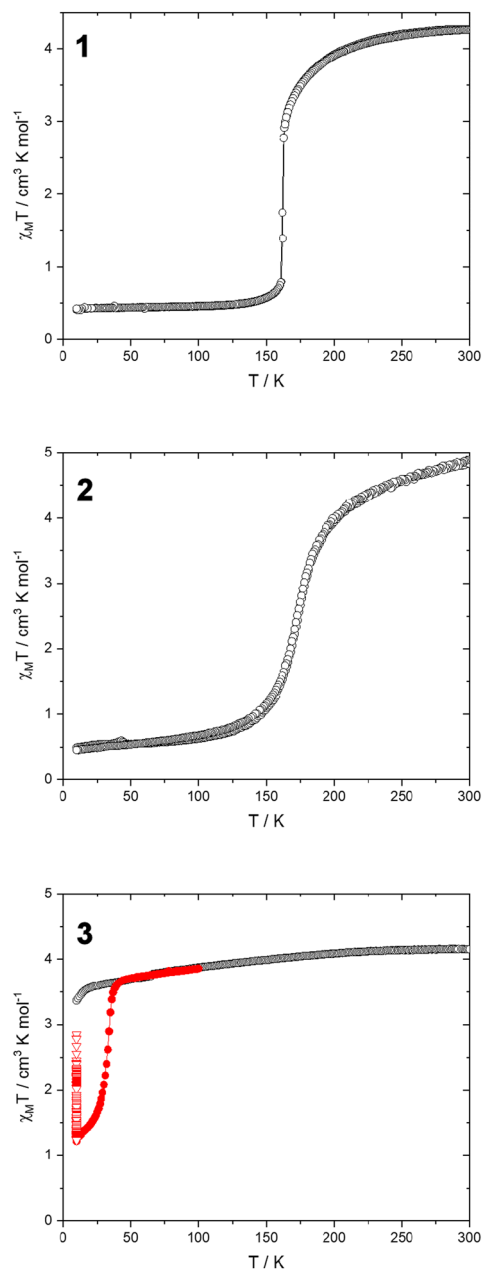


Fig. 1 $\chi_M T$ versus T plots of **1–3**, in the dark before any light irradiation (\circ), under 830 nm light irradiation (∇), in the dark after light irradiation (\bullet).

The magnetic profile upon cooling is found to be identical, indicating an abrupt complete SCO with no hysteresis. Compound **2** shows a similar increase from $0.4 \text{ cm}^3 \text{ mol}^{-1} \text{ K}$ at 100 K before reaching $4.8 \text{ cm}^3 \text{ mol}^{-1} \text{ K}$ at around 250 K, suggesting a more gradual but complete SCO with $T_{1/2} = 172 \text{ K}$. In both **1** and **2**, no thermal quenching was observed upon fast cooling. Neither compound is sensitive to light irradiation at low temperature, showing an inefficient LIESST effect.

In contrast, **3** shows a very gradual decrease from $4.0 \text{ cm}^3 \text{ mol}^{-1} \text{ K}$ at 300 K to $3.7 \text{ cm}^3 \text{ mol}^{-1} \text{ K}$ at 30 K, before declining more sharply at 10 K indicative of zero-field splitting. This suggests little to no SCO in this compound. However, the LS state of **3** can be accessed *via* light irradiation at either 830 or 980 nm (4 mW cm^{-2} was chosen to prevent temperature destabilisation) characteristic of *reverse*-LIESST. The decrease in magnetic susceptibility from 3.5 to $1.2 \text{ cm}^3 \text{ mol}^{-1} \text{ K}$ at 15 K shows that the *reverse*-LIESST is 60% complete after two hours of irradiation (assuming the fully LS state to have a $\chi_M T$ value of around $0.375 \text{ cm}^3 \text{ mol}^{-1} \text{ K}$). *Reverse*-LIESST is extremely uncommon in Fe(III) and to the best of our knowledge there are only a handful of reported examples.^{8,43–45} Heating causes a gradual increase in magnetic susceptibility up to the initial HS curve at 45 K. An additional photocrystallographic study would be needed to identify the phases and their dynamics.

Structural studies

Suitable dark green crystals for SCXRD of **1–3** were prepared from slow diffusion of either CH_2Cl_2 or CHCl_3 with hexane or acetone with Et_2O (Table S3†). PXRD confirms that the crystal structures are reflective of the bulk materials (Fig. S7†). The structures of all complexes are found in the monoclinic $P2_1/c$ space group at all temperatures.

The asymmetric unit of **1–3** contains a 2:1 octahedral complex of the deprotonated naphPren ligand to the Fe(III) center in a *mer* configuration, an iodide anion and single molecule of solvent (Fig. 2 and S6†). The N–H \cdots I interaction is present in all complexes with distances ranging from 2.6–2.9 Å. At 150 K, the Fe(III) centre in **1** has average bond lengths and distortion parameters indicative of the LS state, while in **2**, access to the full LS state requires further cooling

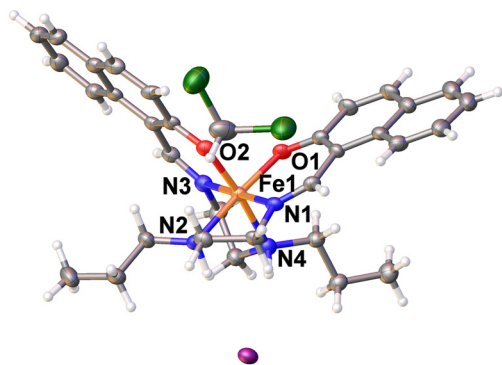


Fig. 2 Asymmetric unit in **1** at 150 K. Ellipsoids are drawn at 50%.

Table 1 Selected bond lengths and octahedral distortion parameters for $[\text{Fe}(\text{naphPren})_2]\text{I-solv}$ complexes where solv = CH_2Cl_2 , **1**, CHCl_3 , **2** and acetone, **3**

	1		2		3		
<i>T</i> (K)	150	200	130	150	200	298	150
Fe1–O _{ave} (Å)	1.89	1.93	1.89	1.89	1.93	1.93	1.93
Fe1–N _{imine} (Å)	1.93	2.06	1.92	1.93	2.05	2.07	2.07
Fe1–N _{amine} (Å)	2.05	2.21	2.06	2.08	2.20	2.22	2.23
Fe1–N/O _{ave} (Å)	1.96	2.06	1.96	1.97	2.06	2.07	2.08
$\Delta\text{Fe–O/N}$ (Å)	0.109		0.117	(298–130 K)			—
Σ (°)	42.6	69.6	42.6	42.4	62.3	69.3	70.7
Θ (°)	125	221	132	137	208	228	232
$\Delta\Sigma, \Delta\Theta$ (°)	27.0, 96		26.7, 96				—
Spin state	LS	HS	LS	mLS	mHS	HS	HS

to 130 K (Table 1).³⁰ Upon warming the bonds elongate and distortion in **1** is observed and plateaus at 200 K, indicating the transition to HS state. In contrast, while **2** starts to level out at 200 K it does not reach the full HS state until 298 K. Upon complete LS to HS crossover, **1** and **2** exhibit an average elongation of the Fe–N/O bonds by 0.11–0.12 Å, and an increase in Σ and Θ of 27° and 96°, alongside an expansion of the unit cell by approximately up to 3–4% (ref. 31, 46 and 47) Unlike the full SCO observed in **1** and **2**, the Fe(III) centre in **3** is HS at 150 K. The structural data are entirely consistent with the magnetic studies reported above.

Apart from the change within the coordination sphere, there are also substantial differences in the N–H \cdots I interactions. While for **2** and **3** the N–H \cdots I interactions are relatively symmetrical and elongate evenly upon SCO in **2**, they are less symmetric in **1** and become increasingly asymmetric upon SCO (Table S3†). However, the most obvious change in **1** and **2** is an order–disorder transition of

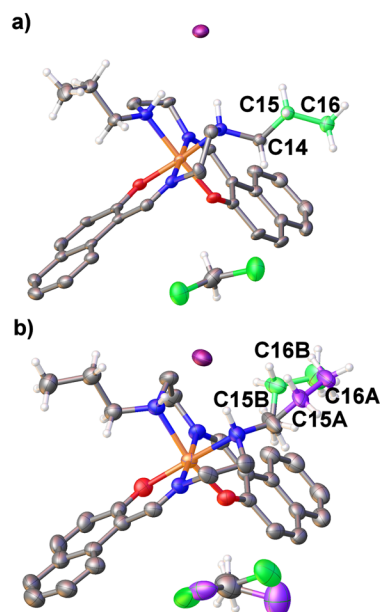


Fig. 3 Order–disorder transition of the propyl substituent and solvent in **1** at a) 150 K and b) 200 K. Ellipsoids are drawn at 50%.

the propyl group that is clearly linked to SCO (Fig. 3 and S8†). Upon heating, we find that the propyl group is disordered over two sites, principally *via* rotation around the N2–C14 bond as observed in the torsion angles. This difference is greatest in **1** and may be factor in the more abrupt SCO observed in this compound. Interestingly, in **3** the Fe–N2–C14–C15 torsion angle is the lowest in the group and as the compound is trapped in the HS state, this suggests that there may be a limit beyond which thermal SCO becomes impossible. Unlike in compounds **2** and **3**, in **1** there is also disorder of the CH₂Cl₂ molecule at 200 K, but the presence of an ordered CHCl₃ molecule in **2** shows that it is disorder in the propyl group that is key to the observation of SCO.

Structural packing

Examining the broader structural features, despite the different lattice solvents, the complexes all pack into 1-D chains along the *b*-axis. The 1-D chain from each structure is generated through a series of N–H···I, I···Cl (or I···H) contacts involving the solvent, and C–H···O interactions (Fig. 4, 5 and S9†). This motif is also supported by several C–H··· π contacts from the naphthyl and propyl groups, resulting in a robust structural motif which is mostly preserved upon SCO. Interestingly, the CH₂Cl₂ molecule in the LS state bridges the Fe(III) spin centres in the 1-D chain *via* C–H···O interactions. However, upon SCO one of the C–H···O interactions is replaced by a weak Cl···O interaction.

A similar interaction is observed in **2** with alternating C–H···O and Cl···O contacts, which weaken upon SCO. These changes in the interactions influence the Fe···Fe distances in

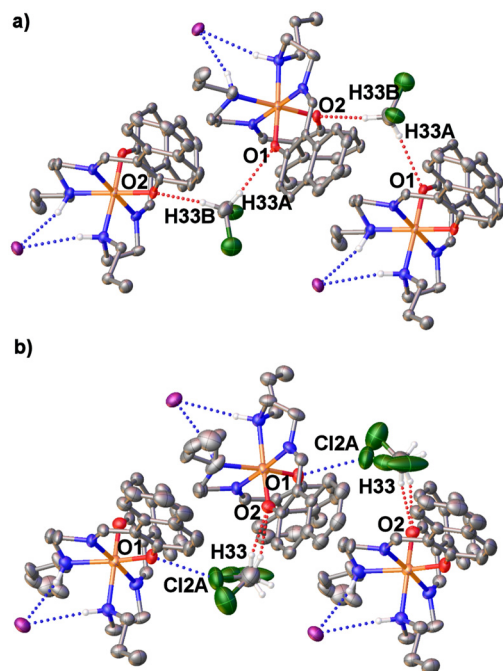


Fig. 5 View along the *b*-axis of the 1-D chain in **1** at a) 150 K and b) 200 K showing the change in the supramolecular interactions involving the CH₂Cl₂ molecule.

the 1-D chain, which become shorter by up to 0.19 and 0.11 Å in **1** and **2**, respectively. It is possible that this difference in **1** and **2** impacts the overall cooperativity and hence the abruptness of SCO. The 1-D chains in **1–3**, are linked into 2-D sheets by C–H··· π interactions involving the naphthyl and propyl groups along the crystallographic *c*-axis (see

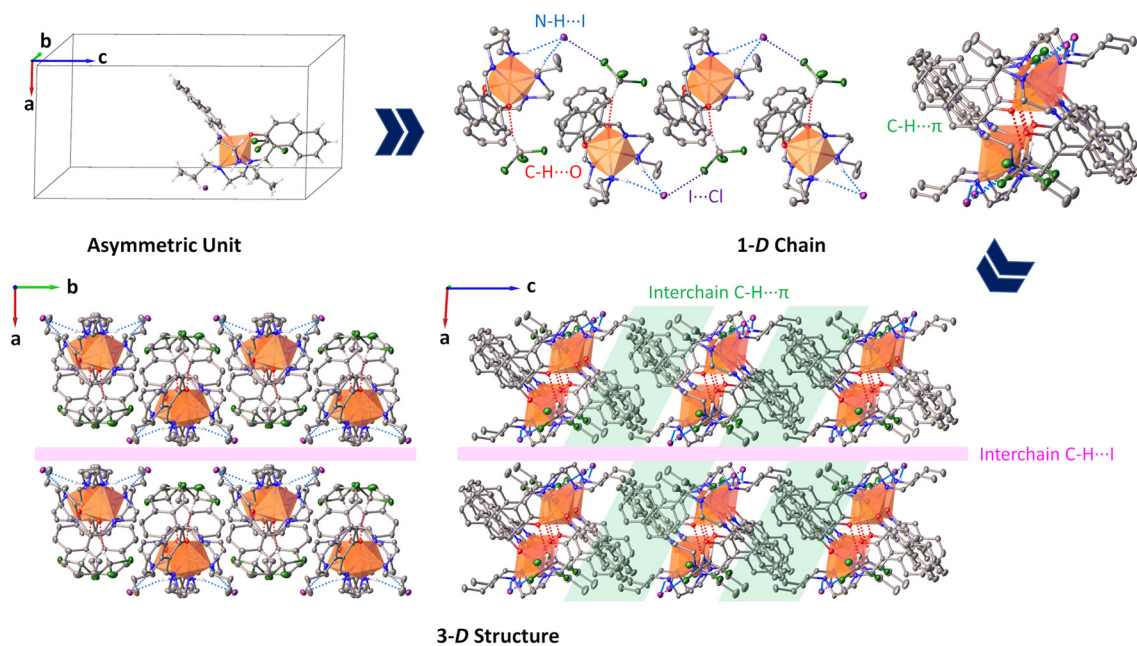


Fig. 4 Schematic illustration of the packing from the asymmetric unit to the final supramolecular 3D structure for [Fe(naphPren)₂]I·CHCl₃ **2** at 150 K. This figure is intended as a guide to the discussion only.

Fig. 4). In addition, relatively weak C–H···I interactions connect the chains along the *a*-axis completing the 3-D structure. It is interesting to note that it is the *a*- and *c*-axes that show the most significant changes upon SCO (0.16–0.56 Å, Table S2†). This suggests that the expansion of the lattice upon conversion to the HS state takes places between the chains and not within them.

Conclusions

We present three solvates of [Fe(naphPren)₂]I which are readily prepared by recrystallization from CH₂Cl₂, CHCl₃ and acetone and suitable antisolvents. Magnetic studies reveal that **1** and **2** exhibit abrupt and moderately abrupt SCO, respectively. In contrast, **3** remains HS at all recorded temperatures. However, it does exhibit *reverse*-LIESST to a hidden LS state with either 830 or 980 nm light, marking a growing trend in Fe(III) SCO chemistry where hidden spin states are accessible in systems that undergo incomplete thermal SCO. The flexibility of the propyl group and subsequent order–disorder transition is intimately associated with SCO in these complexes. The degree of change in the SCO cation-solvent interaction in the 1-D chain, the larger change in the Fe···Fe distances and the additional order–disorder in the CH₂Cl₂ solvent are likely factors in the more abrupt SCO observed in **1** compared with **2**. The current results suggest that further SCO systems with improved properties are waiting to be discovered by extra variations in the alkyl chain in the salRen and naphRen families and further work along these lines is currently in progress.

Author contributions

Theerapoom Boonprab: investigation, formal analysis, data curation, visualization, writing – original draft. Upeksha Habarakada: investigation, formal analysis, data curation. Guillaume Chastanet: investigation, formal analysis, data curation, writing – review & editing. Phimpaka Harding: conceptualization, resources, writing – review & editing, supervision. David J. Harding: conceptualization, resources, writing – review & editing, supervision, funding acquisition.

Conflicts of interest

There are no conflicts to declare.

Acknowledgements

We gratefully acknowledge the National Research Council of Thailand (NRCT) grant number NRCT5-RSA63019-02 for funding. We gratefully acknowledge the award of a Ph.D. Excellence Scholarship by Walailak University to U. H. (Contract No. 01/2019). This research has received funding support from the NSRF *via* the Program Management Unit for Human Resources & Institutional Development, Research and Innovation (grant number: B13F660057).

Notes and references

- 1 P. Gütllich, Y. Garcia and H. A. Goodwin, *Chem. Soc. Rev.*, 2000, **29**, 419–427.
- 2 M. Nihei, T. Shiga, Y. Maeda and H. Oshio, *Coord. Chem. Rev.*, 2007, **251**, 2606–2621.
- 3 A. B. Gaspar, M. Seredyuk and P. Gütllich, *J. Mol. Struct.*, 2009, **924–926**, 9–19.
- 4 D. J. Harding, P. Harding and W. Phonsri, *Coord. Chem. Rev.*, 2016, **313**, 38–61.
- 5 D. J. Harding, W. Phonsri, P. Harding, I. A. Gass, K. S. Murray, B. Moubaraki, J. D. Cashion, L. Liu and S. G. Telfer, *Chem. Commun.*, 2013, **49**, 6340–6342.
- 6 N. Phukkaphan, D. L. Cruickshank, K. S. Murray, W. Phonsri, P. Harding and D. J. Harding, *Chem. Commun.*, 2017, **53**, 9801–9804.
- 7 W. Phonsri, P. Harding, L. Liu, S. G. Telfer, K. S. Murray, B. Moubaraki, T. M. Ross, G. N. L. Jameson and D. J. Harding, *Chem. Sci.*, 2017, **8**, 3949–3959.
- 8 T. Boonprab, S. J. Lee, S. G. Telfer, K. S. Murray, W. Phonsri, G. Chastanet, E. Collet, E. Trzop, G. N. L. Jameson, P. Harding and D. J. Harding, *Angew. Chem.*, 2019, **131**, 11937–11941.
- 9 S. K. Karuppanan, A. Martín-Rodríguez, E. Ruiz, P. Harding, D. J. Harding, X. Yu, A. Tadich, B. Cowie, D. Qi and C. A. Nijhuis, *Chem. Sci.*, 2021, **12**, 2381–2388.
- 10 S. Hayami, K. Hiji, T. Kawahara, Y. Maeda, D. Urakami, K. Inoue, M. Ohama, S. Kawata and O. Sato, *Chem. – Eur. J.*, 2009, **15**, 3497–3508.
- 11 M. Nakaya, R. Ohtani, L. F. Lindoy and S. Hayami, *Inorg. Chem. Front.*, 2021, **8**, 484–498.
- 12 S. Hayami, Z. Z. Gu, M. Shiro, Y. Einaga, A. Fujishima and O. Sato, *J. Am. Chem. Soc.*, 2000, **122**, 7126–7127.
- 13 K. Takahashi, H. B. Cui, Y. Okano, H. Kobayashi, H. Mori, H. Tajima, Y. Einaga and O. Sato, *J. Am. Chem. Soc.*, 2008, **130**, 6688–6689.
- 14 T. Shimizu, Y. Komatsu, H. Kamihata, Y. H. Lee, A. Fuyuhiro, S. Iijima and S. Hayami, *J. Inclusion Phenom. Macrocyclic Chem.*, 2011, **71**, 363–369.
- 15 M. Nakaya, K. Shimayama, K. Takami, K. Hirata, A. S. Alao, M. Nakamura, L. F. Lindoy and S. Hayami, *Chem. Lett.*, 2014, **43**, 1058–1060.
- 16 W. Thammasangwan, P. Harding, S. G. Telfer, A. Alkaş, W. Phonsri, K. S. Murray, R. Clérac, M. Rouzières, G. Chastanet and D. J. Harding, *Eur. J. Inorg. Chem.*, 2020, **2020**, 1325–1330.
- 17 K. Takahashi, K. Kawamukai, M. Okai, T. Mochida, T. Sakurai, H. Ohta, T. Yamamoto, Y. Einaga, Y. Shiota and K. Yoshizawa, *Chem. – Eur. J.*, 2016, **22**, 1253–1257.
- 18 I.-R. Jeon, C. Mathonière, R. Clérac, M. Rouzières, O. Jeannin, E. Trzop, E. Collet and M. Fourmigué, *Chem. Commun.*, 2017, **53**, 10283–10286.
- 19 G. S. Matouzenko, A. Bousseksou, S. A. Borshch, M. Perrin, S. Zein, L. Salmon, G. Molnar and S. Lecocq, *Inorg. Chem.*, 2004, **43**, 227–236.
- 20 G. A. Craig, J. S. Costa, O. Roubeau, S. J. Teat and G. Aromí, *Chem. – Eur. J.*, 2011, **17**, 3120–3127.

- 21 H. J. Shepherd, G. Tonge, L. E. Hatcher, M. J. Bryant, J. V. Knichal, P. R. Raithby, M. A. Halcrow, R. Kulmaczewski, K. J. Gagnon and S. J. Teat, *Magnetochemistry*, 2016, **2**, 9.
- 22 T. Delgado, A. Tissot, L. Guénée, A. Hauser, F. J. Valverde-Muñoz, M. Serezyuk, J. A. Real, S. Pillet, E.-E. Bendeif and C. Besnard, *J. Am. Chem. Soc.*, 2018, **140**, 12870–12876.
- 23 I. C. Berdiell, R. Kulmaczewski, N. Shahid, O. Cespedes and M. A. Halcrow, *Chem. Commun.*, 2021, **57**, 6566–6569.
- 24 N. Suryadevara, A. Mizuno, L. Spieker, S. Salamon, S. Sleziona, A. Maas, E. Pollmann, B. Heinrich, M. Schleberger, H. Wende, S. K. Kuppasamy and M. Ruben, *Chem. – Eur. J.*, 2022, **28**, e202103853.
- 25 D. Chernyshov, M. Hostettler, K. W. Törnroos and H. B. Bürgi, *Angew. Chem., Int. Ed.*, 2003, **42**, 3825–3830.
- 26 M. A. Al-Azzani, F. Al-Mjeni, R. Mitsuhashi, M. Mikuriya, I. A. Al-Omari, C. C. Robertson, E. Bill and M. S. Shongwe, *Chem. – Eur. J.*, 2019, **26**, 4766–4779.
- 27 M. S. Haddad, W. D. Federer, M. W. Lynch and D. N. Hendrickson, *J. Am. Chem. Soc.*, 1980, **102**, 1468–1470.
- 28 M. S. Haddad, W. D. Federer, M. W. Lynch and D. N. Hendrickson, *Inorg. Chem.*, 1981, **20**, 131–139.
- 29 B. Dey, A. Mondal and S. Konar, *Chem. – Asian J.*, 2020, **15**, 1709–1721.
- 30 A. Tissot, P. Fertey, R. Guillot, V. Briois and M. L. Boillot, *Eur. J. Inorg. Chem.*, 2014, 101–109.
- 31 A. I. Vicente, A. Joseph, L. P. Ferreira, M. De Deus Carvalho, V. H. N. Rodrigues, M. Duttine, H. P. Diogo, M. E. Minas Da Piedade, M. J. Calhorda and P. N. Martinho, *Chem. Sci.*, 2016, **7**, 4251–4258.
- 32 F. F. Martins, A. Joseph, H. P. Diogo, M. E. Minas da Piedade, L. P. Ferreira, M. D. Carvalho, S. Barroso, M. J. Romão, M. J. Calhorda and P. N. Martinho, *Eur. J. Inorg. Chem.*, 2018, **25**, 2976–2983.
- 33 P. N. Martinho, A. I. Vicente, S. Realista, M. S. Saraiva, A. I. Melato, P. Brandão, L. P. Ferreira and M. De Deus, *J. Organomet. Chem.*, 2014, **760**, 48–54.
- 34 W. Phonsri, V. Martinez, C. G. Davies, G. N. L. Jameson, B. Moubaraki and K. S. Murray, *Chem. Commun.*, 2016, **52**, 1443–1446.
- 35 T. Boonprab, P. Harding, K. S. Murray, W. Phonsri, S. G. Telfer, A. Alkaş, R. Ketkaew, Y. Tantirungrotechai, G. N. L. Jameson and D. J. Harding, *Dalton Trans.*, 2018, **47**, 12449–12458.
- 36 U. Habarakada, T. Boonprab, P. Harding, K. S. Murray, W. Phonsri, S. M. Neville, M. Ahmed and D. J. Harding, *Cryst. Growth Des.*, 2022, **22**, 4895–4905.
- 37 *Rigaku XRD*, Rigaku Corporation Tokyo, Japan, 2018.
- 38 *CrysAlisPro*, Rigaku Corporation Tokyo, Japan, 2019.
- 39 G. M. Sheldrick, *Acta Crystallogr., Sect. A: Found. Adv.*, 2015, **71**, 3–8.
- 40 G. M. Sheldrick, *Acta Crystallogr., Sect. C: Struct. Chem.*, 2015, **71**, 3–8.
- 41 O. V. Dolomanov, L. J. Bourhis, R. J. Gildea, J. A. K. Howard and H. Puschmann, *J. Appl. Crystallogr.*, 2009, **42**, 339–341.
- 42 R. H. Petty, E. V. Dose, M. F. Tweedle and L. J. Wilson, *Inorg. Chem.*, 1978, **17**, 1064–1071.
- 43 Z. Liu, Z. Yao and J. Tao, *Inorg. Chem.*, 2021, **60**, 10291–10301.
- 44 X. Li, D. Zhang, Y. Qian, W. Liu, C. Mathonière, R. Clérac and X. Bao, *J. Am. Chem. Soc.*, 2023, **145**, 9564–9570.
- 45 R. Díaz-Torres, G. Chastanet, E. Collet, E. Trzop, P. Harding and D. J. Harding, *Chem. Sci.*, 2023, DOI: [10.1039/D3SC01495A](https://doi.org/10.1039/D3SC01495A).
- 46 A. Tissot, R. Bertoni, E. Collet, L. Toupet and M. L. Boillot, *J. Mater. Chem.*, 2011, **21**, 18347–18353.
- 47 C. F. Sheu, S. M. Chen, G. H. Lee, Y. H. Liu, Y. S. Wen, J. J. Lee, Y. C. Chuang and Y. Wang, *Eur. J. Inorg. Chem.*, 2013, **2**, 894–901.